Mixing of Viscoelastic Fluid Flows in a Coiled Flow Inverter

Vikrant, Vikrant; Topalović, Anis; Monechi, Guido; Alsudani, Ali; Nigam, Krishna D.P.; Padding, Johan T.

DOI
10.1021/acs.iecr.9b05142

Publication date
2020

Document Version
Final published version

Published in
Industrial and Engineering Chemistry Research

I&EC research
Industrial & Engineering Chemistry Research

pubs.acs.org/IECR

Article

Mixing of Viscoelastic Fluid Flows in a Coiled Flow Inverter

Vikrant Verma, Anis Topalović, Guido Monechi, Ali Alsudani, Krishna D. P. Nigam, and Johan T. Padding*

Cite This: *Ind. Eng. Chem. Res.* 2020, 59, 3854−3864

Read Online

ACCESS | Metrics & More | Article Recommendations

ABSTRACT: Despite having the advantage of a secondary flow pattern in coiled tubes, a very high Dean number is required to induce significant mixing in helical coils, usually implying high shear rates. At very high shear rates, polymer fluids with long molecular chains can be damaged. Therefore, in this study, we investigate the enhancement of mixing of a viscoelastic fluid in a coiled tube at low Dean numbers using the concept of a coiled flow inverter (CFI). Viscoelastic flow simulations were performed for CFIs of different curvature ratios, by changing the coil diameter, for a range of Weissenberg numbers (*Wi*) 0−125. An analytical method using velocity streamlines to quantify mixing is presented. The pressure drop per unit length increases with increasing *Wi* number. A more efficient mixing is predicted in the CFI, when compared with a helix of the same curvature ratio for all flow conditions. The mixing in the CFI is improved with an increase in flow rates (Wi). The mixing is enhanced at every bend because of flow inversion in the CFI.

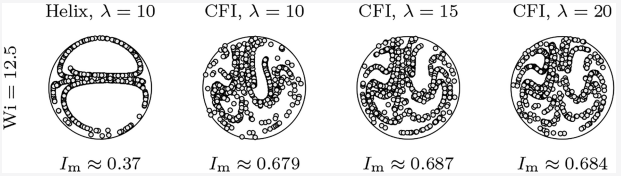

INTRODUCTION

A complete understanding of non-Newtonian fluid flow in complex geometries is of importance in many industrial processes, e.g., for the production of plastics, polymers, and pharmaceuticals to foods. A non-Newtonian fluid does not exhibit a linear relationship between stress and rate of strain. Because of the nonlinear dependence, the analysis of the behavior of the fluid motion of non-Newtonian fluids tends to be much more complicated and subtle in comparison with that of Newtonian fluids.[1,2] A viscoelastic fluid is a common form of non-Newtonian fluid. The flow phenomena that are observable in viscoelastic fluids cannot be predicted by the Navier−Stokes equations using simple viscous stress terms. The complexity of viscoelastic fluid flow is due to the presence of elastic terms that depend on the fluid's flow history, which leads to difficulties with computing the velocity field of viscoelastic fluids even in a relatively simple configuration.[3,4] In general, the velocity profile of a laminar fully developed Newtonian fluid flow through a pipe exhibits a parabola-like profile. In contrast, the flow behavior of a non-Newtonian fluid has many facets. Among them are a shear-rate dependence of the shear viscosity, leading to different (often more plug-flow like) velocity profiles, the presence of normal stress differences, high resistance to elongational deformation, and memory effects associated with the elasticity of the material.[5] Many studies theoretically and experimentally revealed the flow behavior of viscoelastic fluids in simple geometry configurations; the early developments in the numerical analysis of viscoelastic flows are critically reviewed in the book by Bird et al.[5] The viscoelastic fluid poses a characteristic material time scale, i.e., a time scale necessary to relax into a stress-free state after a sudden deformation. The ratio between the material time scale and the time scale of the flow is indicated by the dimensionless Weissenberg number (*Wi*). While *Wi* vanishes for Newtonian fluids, it is on the order of 1 or 10 for many polymer flows of interest. The challenge for numerical models is for a very high *Wi*, known as the High Weissenberg Number Problem or HWNP, which is discussed in detail in Crochet et al.[3] The HWNP is now partially resolved, in that high-Wi numerical solutions have been reported over the years for a variety of flow problems.[6−9] A review by Bird et al.[10] gives a complete list of existing viscoelastic models.

In this paper, we will focus on mixing. Mixing of viscoelastic fluids is important in a variety of industrial applications such as processing of polymer solutions and melts.[11,12] One of the foremost approaches to increase fluid mixing is the use of coiled tubes. The working principle of coiled tubes and reasons for their enhanced performance are well established and as follows: (a) generation of a secondary flow due to unbalanced centrifugal forces; (b) enhanced cross-sectional mixing; (c) a reduction in axial dispersion; (d) improved heat-transfer; and (e) an improved mass-transfer coefficient.[13] The secondary flow pattern was first described by Dean[14,15] and is known as Dean vortices. Dean observed that for a given pressure drop,

Special Issue: Characterization and Applications of Fluidic Devices without Moving Parts

Received: September 18, 2019
Revised: February 6, 2020
Accepted: February 10, 2020
Published: February 10, 2020

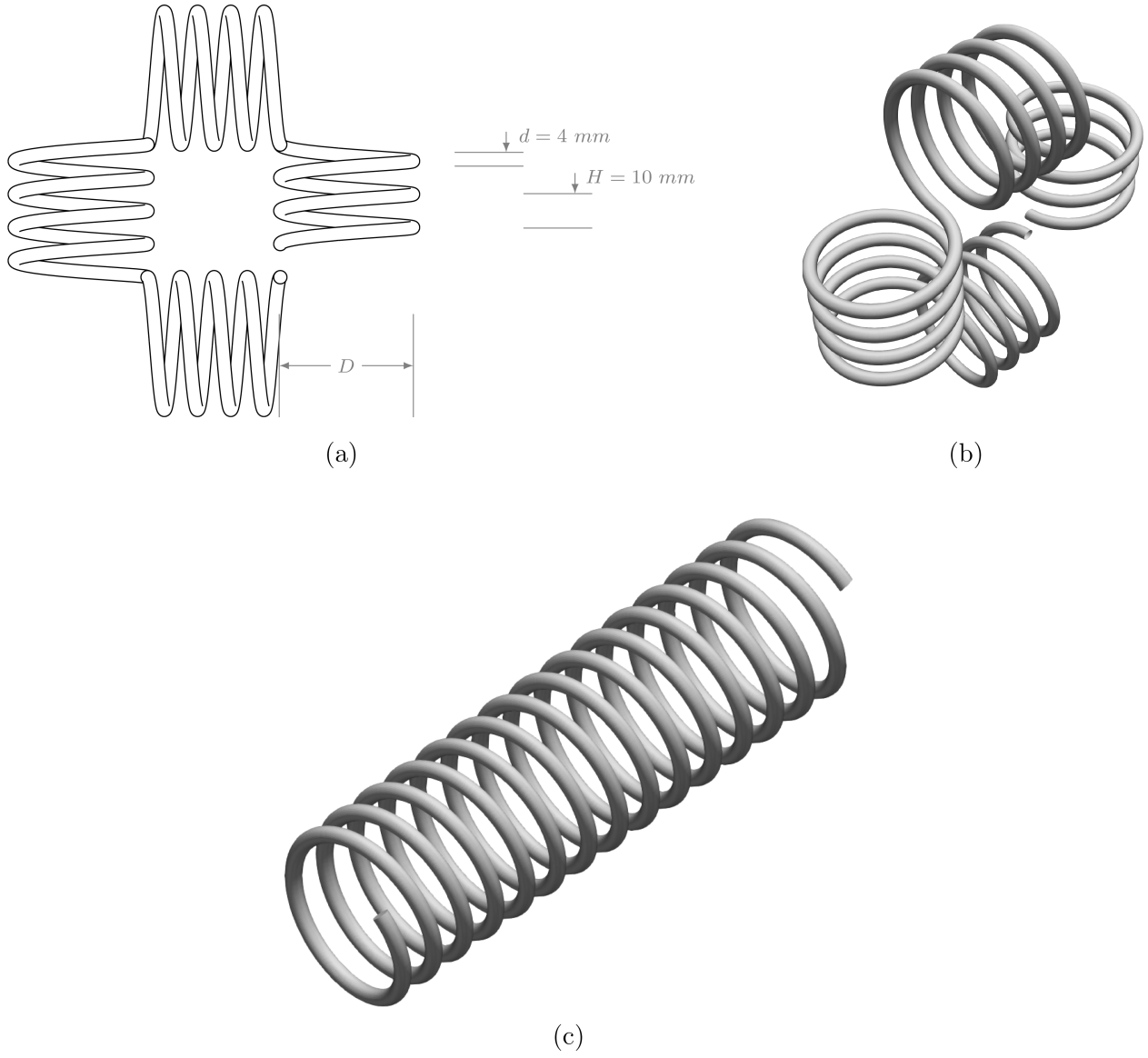

Figure 1. (a) Sketch of the CFI geometry, where d is the diameter of the tube; D, the diameter of the coil; and H, the pitch between the coils. (b and c) Three-dimensional views of the computational geometries for the CFI and helix, respectively. The helix is of a tube length equivalent to that of the CFI.

the volumetric flow rate in a curved tube was less than that in a straight tube.[15] The secondary flow dissipates additional kinetic energy, thus increasing the resistance to flow. The strength of the secondary flow depends on the curvature of the surface. Named after Dean, the flow through a curved channel is quantified by the dimensionless Dean number (De), which is analogous to the Reynolds number (Re) in straight tubes. The Dean number accounts for the effect of curvature ratio and is defined as $De = Re/\sqrt{\lambda}$, where λ is the curvature ratio of the coiled tubes. Numerous studies[13,16−24] have been carried out to understand transport phenomena in coiled tubes that concern steady and transient flows. Several researchers[25−29] have investigated the influence of various parameters on the mechanism of polymerization in coiled tube reactors. Despite having the advantages of a secondary flow pattern in a coiled tube, a careful analysis of the data shows that a very high Dean number (De) is required to induce significant mixing in a cross-sectional plane, usually implying a high shear rate, which can cause long molecular chains to rip. The mixing efficiency in a curved tube is a complex function of the Reynolds number, Schmidt number, curvature ratio, and tube pitch, therefore, the relative effectiveness of a helical tube is quite complicated compared to that of a straight tube.[30] Mansour et al.[31−33] studied a broad range of Reynolds numbers and showed that there are two optimal values of Reynolds number (Re = 20−60 and Re = 350−1000) which lead to excellent mixing conditions between the fluids. For the lower range of Reynolds numbers, strengthening of the Dean vortices enhances mixing. An increase in Reynolds number leads to a more intense vortex structure, improving convective mixing; however, it reduces the residence time of the liquids. To increase the mixing efficiency even at low Dean number, Saxena et al.[34] introduced a new concept of a helical coil, termed the coiled flow inverter (CFI). As shown in Figure 1, the geometrical configuration of a CFI consists of 90° bends in a helical coil, with equal arm length before and after the bend. The secondary flow generated in this device continuously changes direction due to the change in direction of the centrifugal forces caused by

https://dx.doi.org/10.1021/acs.iecr.9b05142
Ind. Eng. Chem. Res. 2020, 59, 3854−3864

bending of a helical coil. The plane of vortex formation rotates with the change in the direction of the centrifugal force by the same angle. A sharp 90° bend in the CFI increases mixing between the fluid elements of different age groups, which provides a more uniform residence time distribution and more uniform temperature distribution within the CFI.[35] The CFI shows enhanced mixing performance without any moving parts and no fixed inserts.[36,37] In coiled tubes and coiled flow inverters, different trends of mixing were shown as a result of varying Reynolds numbers due to the changing nature of Dean vortices.[37]

Zhou and Shah[38] and Naphon and Wongwises[39] performed extensive and critical reviews of theoretical and experimental studies of flow in curved pipes. When these works are reviewed, it is understood that there is only a limited knowledge for non-Newtonian fluids flowing through coils, in particular on the effects of the viscoelasticity of the fluid. Results from studies show that the non-Newtonian fluid can itself also generate a secondary flow, which is in the same plane as the secondary flow due to the centrifugal force.[40−43] Saxena et al.[44] studied the residence time distribution (RTD) of non-Newtonian fluid flow in helical coils. Other researchers[25,45] experimentally studied the dispersion of polymer solutions in coiled tubes. However, only experimental studies have been performed for non-Newtonian fluid flow in coiled geometries.

The resistance to flow through curved tubes, i.e., the pressure drop, can be quantified by the friction factor. The friction factor for a fluid, Newtonian or non-Newtonian, flowing through a helical coil is larger than that for the same fluid flowing through a straight tube under the same conditions.[35] Several other studies[37] reported the flow behavior of Newtonian fluids in coiled tubes. Mridha and Nigam[36] studied the CFI as an inline mixer for Newtonian fluids. The characteristics of non-Newtonian fluids in CFIs have not been investigated in detail. Agrawal et al.[46−48] presented a series of papers on power-law fluids in a circular curved tubes under laminar flow conditions. Singh et al.[35] studied a power law fluid in a CFI and limited the discussion to pressure drop and friction factors. Mandal et al.[49] studied numerically polystyrene synthesis in a coiled flow inverter. However, no study on the mixing characteristics of viscoelastic fluid flow has been reported to date. Therefore, in this computational study, we investigate the flow phenomena and quantify the efficiency of mixing of viscoelastic fluids in a CFI. An analytical approach to quantify mixing from the fluid velocity fields is presented. Simulations were performed using `foam-extend`. Details on simulation settings are given in the Simulation Settings sections, and the approach to quantify mixing is given in the Post-Processing: Quantification of Mixing section. First, a mesh sensitivity study is performed for the CFI and helix geometry. Then, a parametric study for the CFI is presented at different flow conditions. The pressure drop, friction factor, and mixing properties are compared for CFI's for different curvature ratios. A comparison between a CFI and helical geometry for a curvature ratio of 10 is presented. The effects of the sequential bends on mixing in a CFI are compared. We end with our conclusions.

COMPUTATIONAL FLUID DYNAMICS

We consider incompressible and isothermal flow of a shear-thinning polymeric fluid. In the following, we will describe the governing equations for the fluid and the simulation settings.

Governing Equations. We solve the momentum and continuity eqs 1a and 1c, where the fluid stress is described by the FENE-P constitutive model[50] for a Newtonian solvent and single polymeric solute.[51] This gives rise the usual problem of finding the velocity field $\mathbf{u}(t, \mathbf{x}) \in [0, T] \times \mathbf{\Omega}$, pressure field $p(t, \mathbf{x}) \in (0, T) \times \mathbf{\Omega}$, and positive-definite polymeric stress $\boldsymbol{\tau}_p(t, \mathbf{x}) \in [0, T) \times \mathbf{\Omega}$ such that

$$\partial_t \mathbf{u} + \rho \operatorname{div} \mathbf{u} \otimes \mathbf{u} - \eta_s \Delta \mathbf{u} = -\operatorname{grad} p + \operatorname{div} \boldsymbol{\tau}_p + \mathbf{f} \tag{1a}$$

$$z\boldsymbol{\tau}_p + \lambda_F \overset{\nabla}{\boldsymbol{\tau}}_p = 2a\eta_p \mathbf{D} \tag{1b}$$

$$\operatorname{div} \mathbf{u} = 0 \tag{1c}$$

where

$$z = 1 + \frac{3a + \frac{\lambda_F}{\eta_p} tr\, \boldsymbol{\tau}}{l^2}$$

for some shorthand parameter $a := (1 - 3/l^2)^{-1}$ and the deformation rate tensor $\mathbf{D} := 1/2(\operatorname{grad} \mathbf{u} + \operatorname{grad} \mathbf{u}^T)$ on an open, bounded domain $\mathbf{\Omega} \subset R^3$ with a Lipschitz-continuous boundary $\delta\mathbf{\Omega}$.[52] Here p is the hydrostatic pressure; ρ, the volumetrically averaged density, $\boldsymbol{f} \in [0, T] \times \mathbf{\Omega}$, a forcing term; η_s, the viscosity of the Newtonian solvent; $\boldsymbol{\tau}_p$, the deviatoric stress tensor of the polymeric solute, which is modeled as having a single relaxation mode with relaxation time λ_F and zero-shear viscosity η_p; and l^2, the finite molecular extensibility parameter. ∂_t denotes the time derivative; Δ, the Laplacian; $\overset{\nabla}{\circ}$, the upper-convected time derivative, i.e.

$$\overset{\nabla}{\boldsymbol{\tau}}_p := \partial_t \boldsymbol{\tau}_p + (\mathbf{u}\cdot\operatorname{grad})\boldsymbol{\tau}_p - (\operatorname{grad} \mathbf{u})\cdot\boldsymbol{\tau}_p - \boldsymbol{\tau}_p\cdot\operatorname{grad} \mathbf{u}^T$$

and tr○, the tensor trace operator.

In this study, eq 1 is solved with the open-source `viscoelasticFluidFoam` solver,[53] which abstracts away implementational details in a mathematically intuitive way. By virtue of the DEVSS (Discrete Elastic Viscous Stress Splitting),[54] eq 1a is rewritten to the form

$$\partial_t \mathbf{u} + \rho \operatorname{div} \mathbf{u} \otimes \mathbf{u} - (\eta_s + \kappa)\Delta \mathbf{u} = -\operatorname{grad} p + \operatorname{div} \boldsymbol{\tau}_p + \mathbf{f} - \kappa \Delta \mathbf{u}$$

for a calibration constant $\kappa \in R$, such that the $\kappa\Delta\mathbf{u}$ term prevents the unbounded exponential growth of the stress tensor components and thereby a loss of positive definiteness.[53,55,56] Due to the imposed requirement of incompressibility, there is no variation in density to link to pressure, and the computation of eq 1a is decoupled using a hybrid segregated solution algorithm based on the SIMPLE (Semi-implicit Method for Pressure Linked Equations)[57] and PISO (Pressure-Implicit with Splitting of Operators)[58] algorithms. Multiple iterations can be performed per time step to increase solution accuracy.[53,59] The arising discretization is implemented verbatim using the mathematical operator abstractions of `foam-extend 4.x` used in the `viscoelasticFluidFoam.c` solver, barring some efficiency optimizations.[60]

The convective terms and time derivatives were discretized with a first-order upwind interpolation scheme and the Euler method, respectively. The Poisson pressure equation was solved using the generalized Geometric/Algebraic Multi-Grid

https://dx.doi.org/10.1021/acs.iecr.9b05142
Ind. Eng. Chem. Res. 2020, 59, 3854−3864

solver (GAMG), and the velocity and stress were solved using the BiCGstab solver with an Incomplete Lower−Upper (ILU) preconditioner. The absolute precision was set to 10^{-6} for all three solvers.

Simulation Settings. A sketch of the CFI considered in this study is shown in Figure 1, where d is the inner tube diameter and H is the distance between two turns (i.e., the pitch). The value of d and H are fixed to 4 mm and 10 mm, respectively. For comparison, CFIs of curvature ratios (i.e., $\lambda := D/d$) of 10, 15, and 20 were studied by varying the coil diameter D to 40, 60, and 80 mm, respectively. The flow inversion takes place after four helical coil turns in each arm with a total of three bends. This is similar to the geometry used by Mridha and Nigam.[36] The comparison of the CFI with a straight helical coil is performed for a curvature ratio of 10, both having the same length and tube diameter.

We characterize the flow by the values of three dimensionless numbers, namely the zero-shear Reynolds number (Re), Dean number (De), and Weissenberg number (Wi), which are defined as

$$Re := \frac{\rho u_{in} d}{\eta_s + \eta_p},\ De := Re\sqrt{\frac{d}{D}},\ \text{and}\ Wi := \lambda_F \frac{u_{in}}{d} \tag{2}$$

where u_{in} is the inlet velocity; ρ, the volumetrically averaged density; and λ_F, the relaxation time of the polymer. η_s and η_p are the viscosities of the Newtonian solvent and the zero-shear viscosity of the FENE-P polymer solute, respectively. Note that λ is used for the curvature ratio, whereas λ_F indicates a fluid property.

The definition of a Weissenberg number Wi requires a regard for both the geometry and selection of the length scale of interest. The Weissenberg number as defined in eq 2 reflects the shear-dominated nature of the flow at hand[61,62] and was chosen over other definitions for its widespread adoption and convenience; note that a Weissenberg number must be derived from nonlinear properties if a local quantification of shear-thinning is required.[62−64]

The selected parameters for the rheological properties of the FENE-P fluid are given in Table 1. Simulations were

Table 1. Rheological Properties of the FENE-P Fluid Used in the Simulations

rheological properties				
ρ	η_s	η_p	λ_F	l^2
10^3 kg/m^3	0.01 kg/m·s	0.99 kg/m·s	1 s	4

performed for different inlet fluid velocities and their corresponding Re, De, and Wi numbers as given in Table 2. The inlet velocity u_{in} is taken to be an independent variable, tuned to reach the desired Weissenberg number Wi, which is swept over to include the most relevant segments of the shear-thinning regime. The solvent viscosity $\eta_s = 0.01$, was chosen so as to maximize the relative viscosity while conveniently defining the total viscosity to be unity.

POST-PROCESSING: QUANTIFICATION OF MIXING

The mathematical characterization of the mixing performance of fluids is subject to several counterintuitive curiosities: if, for example, streamline dispersion patterns are analyzed using a coefficient of variation of concentration, the resulting index is not an adequate norm for the mixing performance of the

Table 2. Derived Velocity Boundary Condition u_{in} per Geometry

cases				
	dimensionless numbers			
λ	Wi	Re	De	u_{in} in m/s
coiled-flow inverter				
10	12.5	0.2	0.063	0.05
	25	0.4	0.126	0.1
	62.5	1.0	0.316	0.25
	125	2.0	0.632	0.5
15	12.5	0.2	0.052	0.05
	25	0.4	0.103	0.1
	62.5	1.0	0.258	0.25
	125	2.0	0.516	0.5
20	12.5	0.2	0.045	0.05
	25	0.4	0.089	0.1
	62.5	1.0	0.224	0.25
	125	2.0	0.447	0.5
helical geometry				
10	12.5	0.2	0.063	0.05
	25	0.4	0.126	0.1
	62.5	1.0	0.316	0.25
	125	2.0	0.632	0.5

fluid.[65] In the shear-thinning regime in particular, quantification methods based on coefficients of variation or striation area analysis have been reported to give misleading results.[66] Indeed, as stated by Baddley:[67]

The applied literature is dominated by *ad-hoc* methods based on evaluating a summary statistic (e.g., the average distance from a point to its nearest neighbor) with very little statistical theory to support them.

We therefore quantified mixing by measuring the scale of segregation with a dispersion index based on the approach discussed in the book by Diggle;[68] assuming that perfect mixing is equivalent to complete spatial randomness (CSR), deviations from the Poisson distribution can be used to quantify clustering.[69] Unlike Kukukova et al.,[65] which use a dimensional dispersion index similar to the third standardized moment, we propose the use of the Szymkiewicz−Simpson overlap coefficient, i.e.

$$I_m = \frac{|X \cap P(\theta = \mu_X)|}{\min|X|, |P(\theta = \mu_X)|} \in [0, 1] \tag{3}$$

to quantify distribution similarity. Here, X is the frequency distribution of the streamline-to-gridpoint distances to the desired precision and P, the Poisson distribution with its parameter equal to the mean of the set X. The index eq 3 approaches unity for perfect mixedness and can therefore also be used to fit to.

The distribution X is obtained by measuring each of the relative distances from a regular reference grid of m points to the n streamlines cutting through a specific cross-section. Edge effects are therefore negligible by construction as long as the grid is sufficiently fine. The grid size and the number of number of data points, in our case streamlines, is a complex interplay of, among others, distribution resolution, computational time, particle efficacy, and geometry and therefore has to be determined empirically.[69,70] We chose $n = 1000$ streamlines effective to the selected computational grid size. For our cases, we computed the mixing index for different inlet seed sizes and

https://dx.doi.org/10.1021/acs.iecr.9b05142
Ind. Eng. Chem. Res. 2020, 59, 3854−3864

found that, while a large number of inlet seed streamlines leads to a much more convergent mixing index at the inlet, it also results in downstream clustering. Our choice of $n = 1000$ streamlines provides the expected consistence in the dispersion index for the simpler case of the helix. Therefore, for a fair relative comparison of the CFI and the helix under different flow conditions, $n = 1000$ streamlines is chosen as the base case for relative comparison.

The fact that $I_m := 1$ for perfectly randomly distributed spatial data can be used to obtain a geometry and measurement-scale independent normalization coefficient c_{norm} by solving the power regression problem

$$c_{norm}(|X|) := \arg\min_{c^*_{norm}} \left\| I_m(c^*_{norm}, X) - 1 \right\| \tag{4a}$$

$$\text{subject to } c_{norm} \in \boldsymbol{R}_{>0} \tag{4b}$$

for a set of randomly distributed streamline coordinates X to the desired precision. The dependence of the normalization coefficient c_{norm} on the cardinality of X should not be thought of as a weakness; methods that rely upon having a "statistically significant" data set, such as the nearest neighbor method[71] that tests for spatial randomness by measuring the distances in between the streamlines themselves, give results that in our experience cannot be trusted in flows with significant plug flow regions as (1) insufficient resolution of the boundary layer can lead to a disproportionately large loss of streamlines near the pipe wall due to numerical artifacts which, in combination with the lack of verifiability of the assumption of statistical significance, can lead to a meaningless mixing index, and (2) these methods do not account for the clustering of the entire population of streamlines within a particular geometry.

RESULTS AND DISCUSSION

First, we discuss the mesh sensitivity study for pressure drop convergence in the Mesh Sensitivity section. Next, we discuss the effect of pressure drop and friction factor for different flow conditions and for different curvature ratios. Next, mixing is quantified in the CFI and helix for different flow conditions. Finally, the effect of sequential bends on the mixing in the CFI is discussed.

Mesh Sensitivity. To study the effect of the mesh size, we performed simulations on a single coil, i.e., revolution, of a helix in order to reduce computational time. Figure 2 shows a cross-sectional view of the generated mesh. In order to control the mesh, refinement was done over the length of the coil ($n_{axial\text{-}extrusions}$) and the scaling of the number of mesh faces on the inlet ("radial scale"), as shown in Table 3. The sensitivity of the mesh is analyzed by the change in predicted pressure drop across the geometry, measured at half the axial length of the coil in order to avoid numerical inlet artifacts. Table 3 shows that the pressure drop decreases as the mesh is refined. The most computationally efficient time permissible parameters that sufficiently resolve the boundary layer and are within 5% relative pressure drop error $\delta^{\Delta p}_{rel}$ was the geometry with 1.61×10^5 elements. Correspondingly, this coil mesh scales up to $\approx 1.8 \times 10^6$ elements in the full coiled-flow inverter.

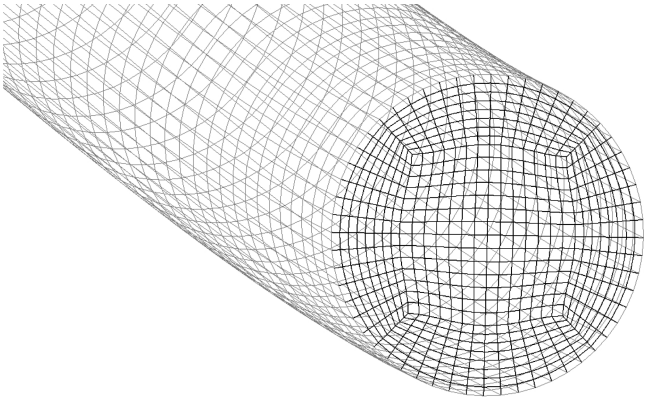

Figure 2. Cross-sectional view of the computational mesh.

Table 3. Mesh Convergence and Sensitivity Study

mesh convergence discretization parameters				
radial scale	$n_{axial\text{-}extrusions}$	$n_{elements}$	Δp [Pa]	$\delta^{\Delta p}_{rel}$ [-] %
	800	1.54×10^6	3.003	
	400	7.68×10^5	3.005	0.067
	250	4.80×10^5	3.096	3.098
	200	3.84×10^5	3.165	5.395
	150	2.90×10^5	3.344	11.34
	100	1.92×10^5	3.653	21.64
0.75	250	2.61×10^5	3.108	3.495
	200	2.09×10^5	3.174	5.686
	150	1.57×10^5	3.290	9.543
	100	1.05×10^5	3.489	16.18
0.6	250	1.61×10^5	3.112	3.623
	200	1.29×10^5	3.176	5.750
	150	9.67×10^4	3.281	9.252
	100	6.44×10^4	3.488	16.137
0.5	250	1.20×10^5	3.119	3.859
	200	9.60×10^4	3.183	5.890
	150	7.20×10^4	3.287	9.467
	100	4.80×10^4	3.490	16.23
0.4	250	8.50×10^4	3.129	4.178
	200	6.80×10^4	3.193	6.309
	150	5.10×10^4	3.297	9.790
	100	3.40×10^4	3.499	16.53

Pressure Drop and Friction Factor. The pressure drop values are given in Table 4 for different Wi numbers. For each given CFI curvature ratio, the pressure drop increases with an increase in Wi number. When comparing the pressure drop for curvature ratios of 10, 15, and 20, the overall pressure drop increases due to an increase in the length of the tube for a high curvature ratio (because the pipe diameter d is fixed). However, the pressure drop per unit length is nearly the same for all CFIs at a given Wi number, as shown in Table 4. Therefore, the curvature ratio that is calculated with regard to a change in coil diameter has no effect on the pressure drop per

Table 4. Pressure Drop Comparison in the CFI for Different Shear Flow Conditions

	$\lambda = 10$		$\lambda = 15$		$\lambda = 20$	
Wi	Δp [Pa]	ΔpL [Pam]	Δp [Pa]	ΔpL [Pam]	Δp [Pa]	ΔpL [Pam]
12.5	32.4	17.1	48.1	17.0	63.9	17.0
25	43.6	23.1	64.3	22.7	85.5	22.8
62.5	66.2	35.0	96.6	34.1	129	34.4
125	95.4	50.8	136	48.1	178	47.5

https://dx.doi.org/10.1021/acs.iecr.9b05142
Ind. Eng. Chem. Res. 2020, 59, 3854−3864

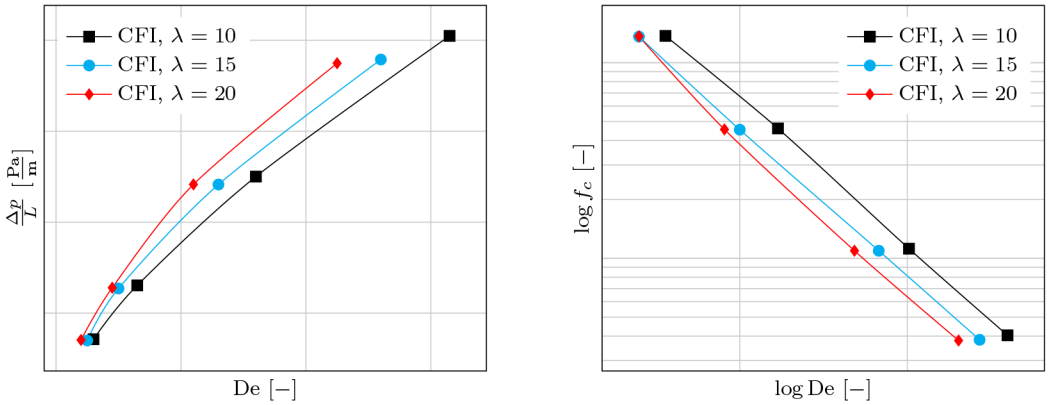

Figure 3. (a) Pressure drop per unit length as a function of Dean number. (b) Log−log plot of the friction factor as a function of the *De* number, compared to CFI curvature ratios of 10, 15, and 20.

unit length for a given flow rate. However, other studies have shown that the pressure per unit length is influenced by curvature ratios when calculated with regard to a change in tube diameter. Due to computational limitations, the effect of curvature ratio change with regard to the tube diameter is not considered in this study. When comparing the CFI with the helix of same tube diameter and curvature ratio ($\lambda := 10$), the pressure drops do not show a significant difference. For a Newtonian fluid flow, an increase of 2−7% in pressure drop in the modified coiled geometry was reported[72] when compared with a helical coil. The absence of an increase in pressure drop in a CFI is promising to process viscoelastic fluids without any additional pumping costs. In the next section, we will discuss how a significant enhancement in mixing is predicted in the CFI compared to the helix.

Figure 3a shows the pressure drop per unit length in the CFI on a log−log plot for varying Dean numbers, compared for CFI curvature ratios of 10, 15, and 20. The pressure drop per unit length increases with an increase in Dean number and decreases with an increase in curvature ratio. It is important to note that the pressure drop per unit length, as a function of the Wi number, does not have any significant effect, as shown in Table 4. Since the De number is calculated from the curvature ratio (see eq 2), a different De number is obtained for a given value of the Wi number. Corresponding to the pressure drop, the friction factor is calculated from the definition of Fanning friction factor. The friction factor represents the resistance to flow and is the ratio of the wall shear stress per unit mass to the kinetic energy head of the fluid.[73] Figure 3b shows the friction factor as a function of Dean number. The friction factor decreases with an increase in Dean number. It is also observed that the friction factor decreases with an increase in curvature ratio. This is due to the fact that the secondary flow becomes less effective with an increase in curvature ratio due to weaker centrifugal force. For Non-Newtonian fluids, Singh et al.[35] also observed a decrease in friction factor with an increase in curvature ratio. They also observed that the friction factor in a CFI is 5 times lower in the case of non-Newtonian fluid flow compared to that of water. The reason is the reduction in viscosity of a shear thinning fluid, which becomes stronger at a higher value of n (power law index). We attribute a similar reason for the reduction in friction factor for our viscoelastic fluid, which is also shear-thinning. For a helical coil, Pimenta and Campos[74] have found that the friction factors in non-Newtonian fluids decrease with an increase of the shear-thinning behavior and seem to increase when the elastic behavior increases.

Mixing Characteristics. Mixing is an important characteristic of coiled geometries, which is generally quantified by introducing a tracer in the fluid. In this study, we presented an analytic approach to the quantification of mixing. The details to calculate the mixing index is given in the postprocessing section. A number of points are defined at the inlet as a starting point of streamlines, which are traced through the geometry. The dispersion of those points by the flow can be used to quantify the quality of mixing. The mixing index I_m can be calculated from the distribution of streamline/tracer points at any cross-sectional plane. To test the effect of the initial location of streamline points at the inlet, five different locations at the inlet are tested, as shown in the top-left of Figure 4 for a thousand streamlines. The corresponding dispersion of streamlines is measured at the outlet cross section with the mixing index (I_m), where the bottom-left plot corresponds to

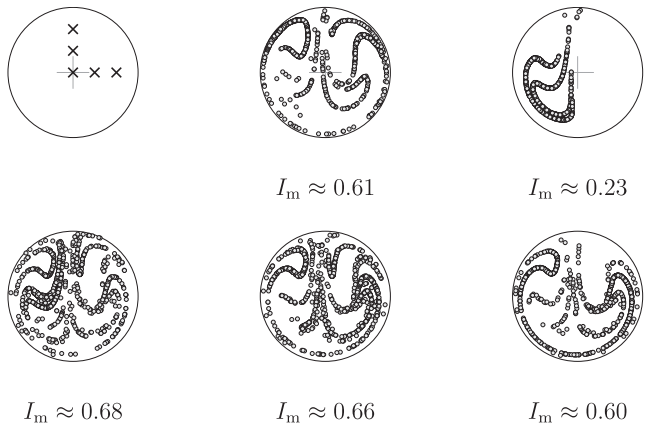

Figure 4. Representation of streamline points for chosen locations at the inlet cross section (top row, left) and the corresponding distributions of streamline points at the outlet. The bottom-left plot corresponds to the center inlet point. The top-central and top-right plots correspond to the locations of the vertical points. Simmilarly, the bottom-central and bottom-right plots correspond to the horizontal points, respectively.

https://dx.doi.org/10.1021/acs.iecr.9b05142
Ind. Eng. Chem. Res. 2020, 59, 3854−3864

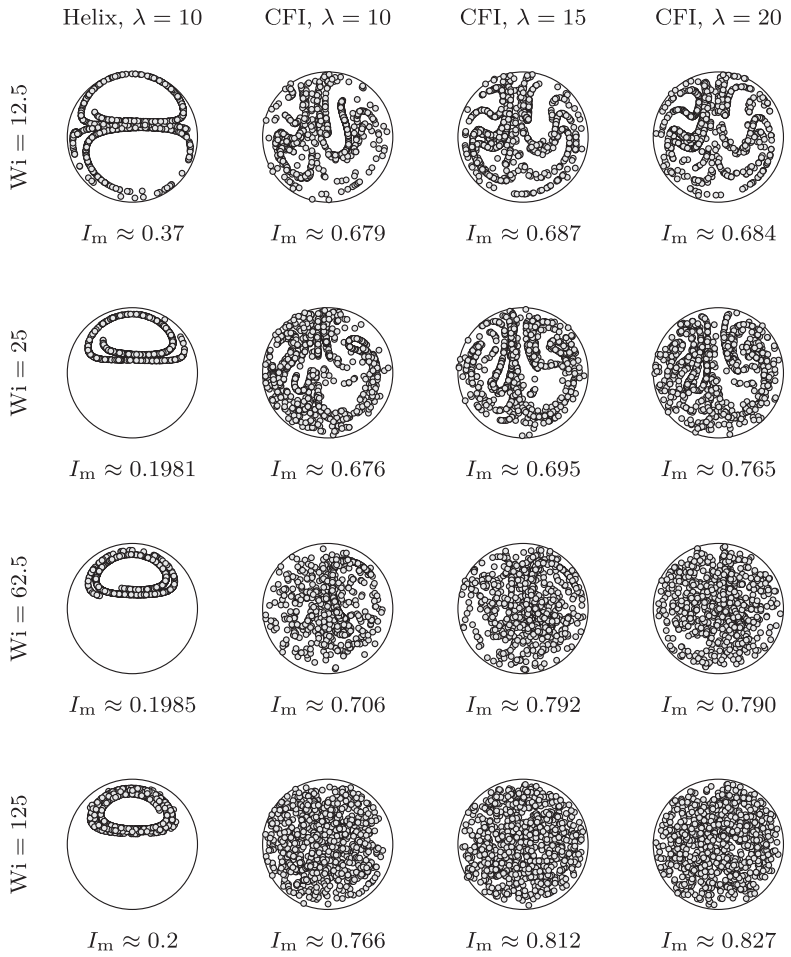

Figure 5. Distribution of streamline points at the outlet of the helix and CFI geometries. Rows represent flow at different *Wi* numbers. The columns represent different geometries at different curvature ratios λ. The value of I_m represents the corresponding mixing index; a value closer to 1 indicates better mixing (i.e., the distribution becomes closer to complete spatial randomness).

the center inlet point. The top-central and top-right plots correspond to the locations of the vertical points. Similarly, the bottom-central and bottom-right correspond to the horizontal points, respectively.

Figure 4 shows that the location of inlet streamlines has a significant effect on dispersion at the outlet. As the inlet point moves toward the wall in the horizontal direction, the mixing index decreases. A maximum of the mixing index is predicted to occur when the inlet tracer point is chosen near the center. The difference in mixing index when moving about the cross-sectional plane is to be expected; the mixing is an interplay of the centrifugal force in the horizontal direction and the velocity profile in general. The centrifugal force on fluid elements affects the dispersion in the horizontal direction. The formation of Dean vortices promotes, due to their symmetric nature, higher dispersions when the inlet point is chosen to be near the center. Therefore, the top-right seed is located in an area where the secondary flow velocity gradient is low and as a consequence of that has a low I_m. The center was chosen as the inlet seed for the subsequent discussion as it is the most neutral point throughout the parameter sweep of Weissenberg numbers for the relevant direction.

Figure 5 shows the cross-sectional view of the dispersion streamline points at the outlet for different *Wi* numbers (different rows) and for the CFI of curvature ratios 10, 15, and 20 (different columns). For comparison, the helix with a curvature ratio of 10 is added. For the helix, the streamline points follow the profile of the Dean vortices. For the helix, the distribution in streamline points is nearly similar for *Wi* = 25, 62.5, and 125 with an I_m = 0.2. The value of the mixing index corresponding to *Wi* = 12.5 is a consequence of the streamlines being dispersed more in the radial direction, moving to the opposite vortices depicted in Figure 5. This is attributed to the residence time being higher at lower *Wi* numbers. Therefore, the residence time has a stronger effect on the mixing index compared to vorticity in helix geometries. Ranade and Ulbrecht[22] reported that in the case of non-Newtonian fluids, the dependence of the apparent viscosity on shear rate changes the velocity distribution over the tube cross-section, which in turn affects the residence time distribution and hence the mixing. Mishra and Gupta[21] observed that, for the case of Newtonian fluid flows, a high Dean number is necessary for mixing to take place in helical coils. Our simulations for the helical geometry show that flow rates affect viscoelastic fluid mixing less than Newtonian fluid mixing. For the case of the CFI, the flow inversion promotes better mixing of viscoelastic fluids, as shown in Figure 5. At a low *Wi* of 12.5 and a curvature ratio of 10, the mixing index is lower for the helix compared to the CFI. This shows that even at a low *Wi* number the inversion of flow in a viscoelastic fluid has a significant effect on the radial dispersion. A detailed discussion of the CFI at low *Wi* is given in the next subsection. As the

https://dx.doi.org/10.1021/acs.iecr.9b05142
Ind. Eng. Chem. Res. 2020, 59, 3854−3864

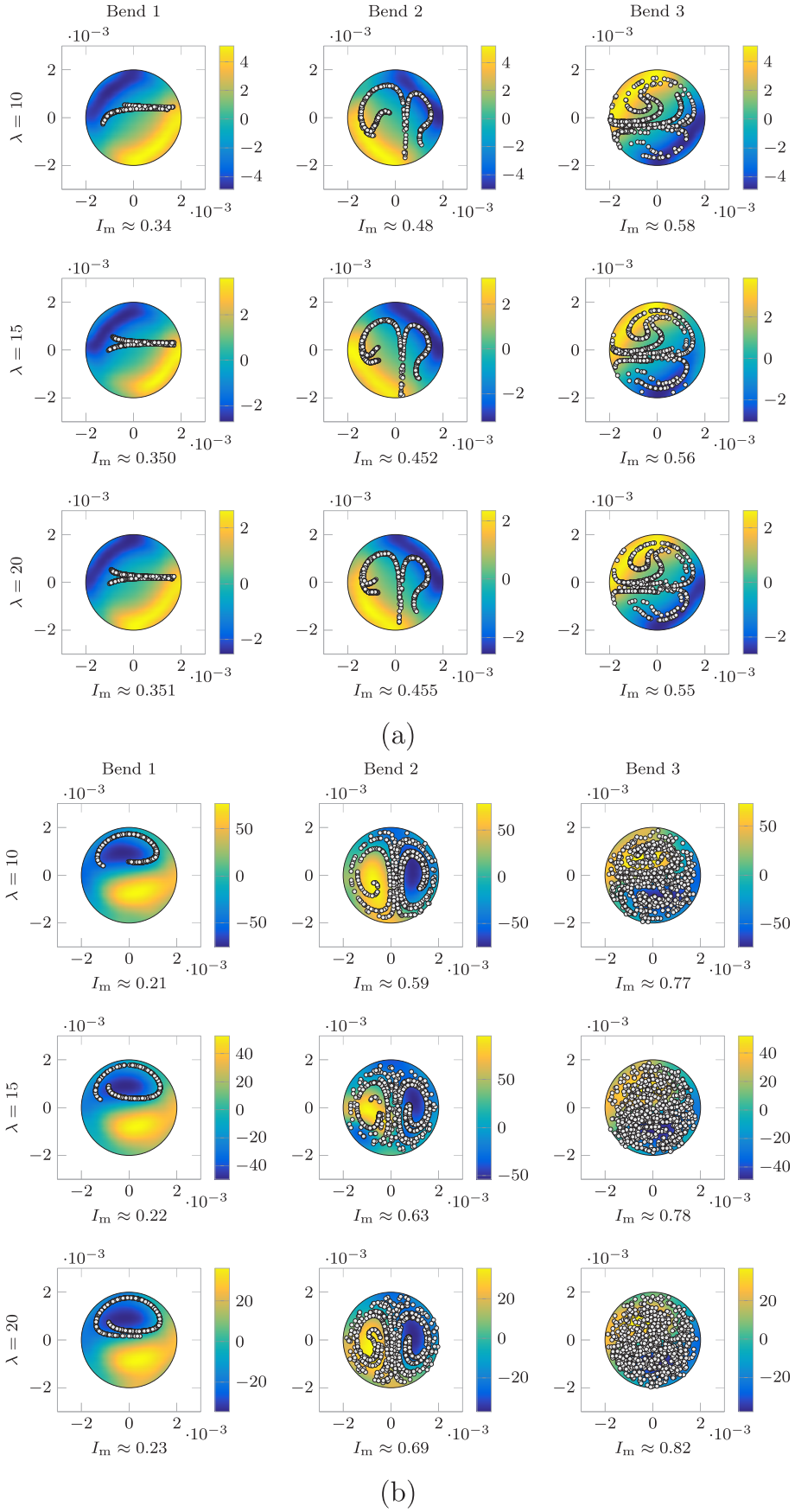

Figure 6. Effect of sequential bends in a CFI for different curvature ratios for (a) Wi = 12.5 and (b) Wi = 125. The secondary flow vortices are shown in color, and the points indicate the distribution of streamlines. Axis dimensions are in m and vorticity (colormap) in rot/s.

https://dx.doi.org/10.1021/acs.iecr.9b05142
Ind. Eng. Chem. Res. 2020, 59, 3854−3864

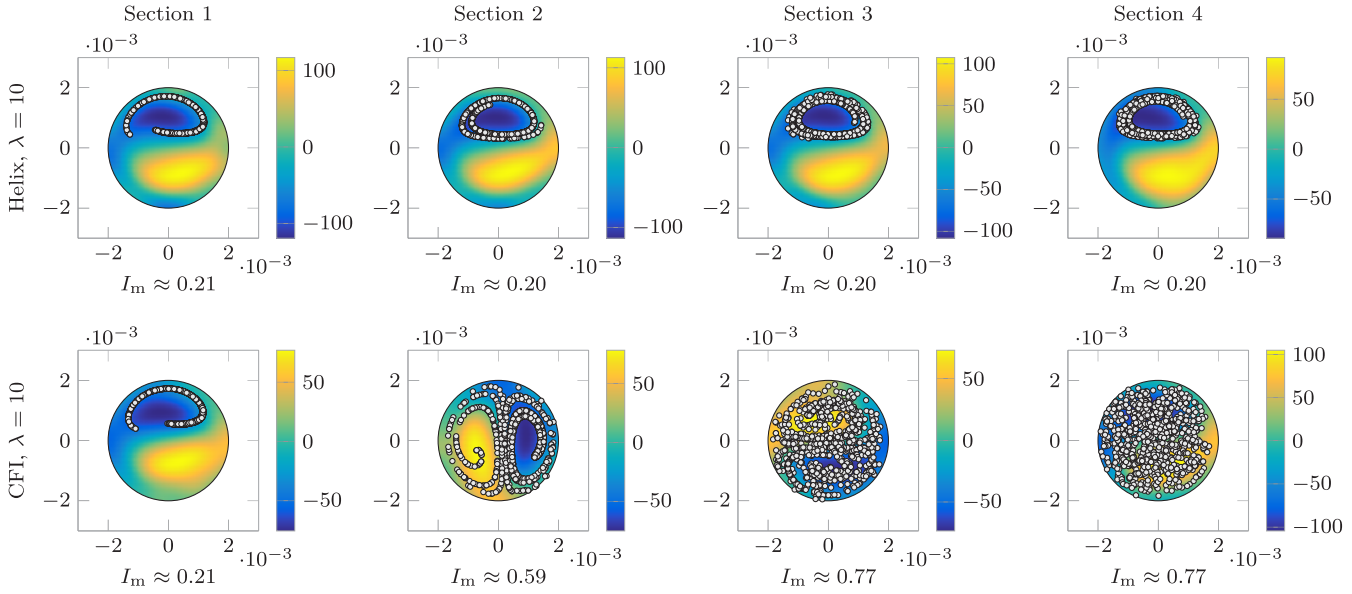

Figure 7. Comparison between the CFI bends and equivalent helix lengths for Wi ≔ 125 showing the effect of CFI bends on the vorticity and streamline dispersion. Axis dimensions are in m and vorticity (colormap) in rot/s.

Weissenberg number increases, the mixing increases for the CFIs of all curvature ratios. In conclusion, Figure 5 clearly shows that the distribution of streamline points is more uniform, and a better mixing is achieved in the CFI as the flow rate of viscoelastic fluid is increased.

When comparing the CFI geometries with different curvature ratio, the mixing index increases with curvatio ratio. A significant enhancement in mixing is predicted when moving to a higher curvature ratio of 15 from a ratio of 10 at a high *Wi* number. When comparing curvature ratios of 15 and 20 at a given *Wi* number, nearly the same mixing index is predicted. Kumar et al.[30] discussed the effect of the lower coil curvature ratio resulting in improved mixing due to the increased centrifugal effects. In principle, for a smaller curvature ratio, the intensity of the secondary flow is very high (due to the higher centrifugal force), in comparison to that for a higher curvature ratio. The high intensity of the secondary flows promotes better mixing. However, the increase in curvature ratio, i.e., by increasing the coil diameter, requires a longer tube length for the same number of turns. The effective increase in length of tube also allows for a higher residence time, resulting in better mixing. Therefore, mixing is a function of both vorticity as well as residence time. The increase in curvature ratio by virtue of a change in tube diameter can be chosen as such to provide the same equivalent tube length but leads to a different radial dispersion and is not considered in this study. A detailed discussion on curvature ratios is presented in the following subsection, where we discuss the combined effect of sequential bends.

Effects of Sequential Bends. Figure 6 shows the effect of sequential bends in the CFI for *Wi* numbers 12.5 and 125 for curvature ratios of 10, 15, and 20. In these subfigures, the intersection of the streamlines with the outlet is shown along with the secondary flow vortex intensity on a color scale. It is observed that the magnitude of the secondary flow vortices decreases with an increase in curvature ratio for a given *Wi* number. The high magnitude of vortices at a small curvature ratio shows that the intensity of the secondary flow is very high due to a high centrifugal force on the fluid element. The same magnitude of flow vortices at each bend shows that the intensity of secondary flow is nearly the same; however an inversion of flow is taking place at each bend. The circular patterns are flipped at each bend which changes the direction of the vortices. The location of the vortices is the same for all curvature ratios, irrespective of *Wi* number. For a high *Wi* of 125 the vortices are symmetric and more pronounced. The 90° flipping of vortices due to flow inversion in the CFI is evident at high Weissenberg numbers for all the curvature ratios.

When comparing the distribution of streamline points in the cross-section at each bend, the distribution perfectly follows the vortices at *Wi* = 125, while for a lower Weissenberg number of *Wi* = 12.5 the points are clustered for a curvature ratio of 10, and a more wide distribution of streamline points occurs for curvature ratios of 15 and 20. Interestingly, for all curvature ratios and *Wi* numbers studied, the distribution of streamlines does not show a significant difference at each bend. This shows that a change in curvature ratio with regard to a change in coil diameter does not have a significant impact on radial mixing at a low *Wi* number of 12.5 as shown in Figure 6a. In Figure 6b, the distribution of points follows the contours of the vortices at the first bend, and for the second and third bends the streamline points distribute uniformly over the vortices. The most significant enhancement of mixing in the CFI takes place when the flow is inverted for the second time at bend 2 and, subsequently, at bend 3. From Figure 6, it is clear that coiled-flow inverter bends have a significant effect on the mixing of viscoelastic fluids. When comparing the helix and the CFI for a curvature ratio of 10 and *Wi* of 125 in Figure 7, the CFI shows a symmetric distribution of streamline points at the first bend and uniform distribution at the second and third bends. However, the helix in Figure 7 shows a distribution of streamline points at vortices throughout. The I_m of approximately 0.2 at different tube lenghts (i.e., sections) shows that no axial and radial mixing is taking place. However, for the CFI, even a single bend is effective in increasing radial mixing in a viscoelastic fluid. Other studies on Newtonian fluids[36] show that the mixing performance of a CFI with only one or two flow inversions is very close to the simple, straight

https://dx.doi.org/10.1021/acs.iecr.9b05142
Ind. Eng. Chem. Res. 2020, 59, 3854−3864

helical pipe, and several flow inversions are required to achieve a considerable enhancement of the mixing performance of a CFI over helical pipes. This again confirms that CFIs may be particularly useful for the enhancement of mixing of non-Newtonian fluids.

CONCLUSIONS

In this work, the flow and mixing characteristics of a viscoelastic fluid in a helical coil and CFI are investigated with the help of CFD simulations using the `foam-extend` solver. An analytical solution to quantify mixing using the streamline point is presented. Simulations were performed for CFIs of curvature ratios 10, 15, and 20 for flow rates corresponding to *Wi* numbers 12.5, 25, 62.5, and 125. A comparison between the CFI and helix having a curvature ratio of 10 is reported. The pressure drop per unit length increases with an increase in *Wi* number and follows a power law relation. The pressure drop per unit length is the same for all curvature ratios for a given *Wi* number. However, the pressure drop per unit length increases with an increase in Dean number. Similarly, the friction factor decreases with increase in Dean number and with an increase in curvature ratios of CFI. When comparing mixing in the CFI and helix of curvature ratio 10, the CFI shows better mixing for a given flow rate. The chosen curvature ratios of 10, 15, and 20 do not have a significant effect on mixing characteristics in the CFI. The bends in a CFI have a significant impact on mixing, where mixing of a viscoelastic fluid is enhanced significantly even at the first bend. The mixing is enhanced at each bend, so the mixing efficiency of a CFI increases with an increase in number of bends. In other mixing devices, high shear flow rates are required for proper mixing of viscoelastic fluids. However, at a high shear flow, fluids with very long molecular chains can be damaged. This work shows that a CFI can lead to improved mixing of viscoelastic fluids even for relatively low shear rates.

AUTHOR INFORMATION

Corresponding Author

Johan T. Padding − *Process and Energy Department, Delft University of Technology, Delft, The Netherlands;* orcid.org/0000-0003-4161-0748; Email: j.t.padding@tudelft.nl

Authors

Vikrant Verma − *Process and Energy Department, Delft University of Technology, Delft, The Netherlands*

Anis Topalović − *Process and Energy Department, Delft University of Technology, Delft, The Netherlands*

Guido Monechi − *Process and Energy Department, Delft University of Technology, Delft, The Netherlands*

Ali Alsudani − *Process and Energy Department, Delft University of Technology, Delft, The Netherlands*

Krishna D. P. Nigam − *Department of Chemical Engineering, Indian Institute of Technology, Delhi, India*

Complete contact information is available at: https://pubs.acs.org/10.1021/acs.iecr.9b05142

Notes

The authors declare no competing financial interest.

REFERENCES

(1) Rajagopal, K. Mechanics of Non-Newtonian Fluids in Recent Developments in Theoretical Fluids Mechanics. *Pitman Research Notes in Mathematics Series* **1993**, *292*, 129.

(2) Dunn, J.; Rajagopal, K. R. Fluids of Differential Type: Critical Review and Thermodynamic Analysis. *Int. J. Eng. Sci.* **1995**, *33*, 689.

(3) Crochet, M.; Davies, A.; Walters, K. *Numerical Simulation of Non-Newtonian Flow*; Elsevier: Amsterdam, 1984.

(4) Keunings, R. *Fundamentals of Computer Modeling for Polymer Processing*; Tucker, C. L., III; Carl Hanser Verlag: Munich, 1989; pp 402−470.

(5) Bird, R.; Armstrong, R.; Hassager, O. *Dynamics of Polymeric Liquids*; Wiley Interscience: New York, 1987; p 649.

(6) Brown, R.; McKinley, G. *J. Non-Newtonian Fluid Mech.* **1994**, *52*, 407.

(7) Caswell, B. *J. Non-Newtonian Fluid Mech.* **1996**, *62*, 99−110.

(8) Baaijens, F. Mixed Finite Element Methods for Viscoelastic Flow Analysis: A Review. *J. Non-Newtonian Fluid Mech.* **1998**, *79*, 361−385.

(9) Keunings, R. A Survey of Computational Rheology. *Proceedings of the XIIIth International Congress on Rheology*; British Society of Rheology, **2000**; pp 7−14.

(10) Bird, R.; Wiest, J. Constitutive Equation for Polymeric Liquids. *Annu. Rev. Fluid Mech.* **1995**, *27*, 169.

(11) Elemans, P. *Mixing and Compounding of Polymers*; Manas, I., Tadmor, Z., Eds.; Hanser Publishers: Munich, 1994.

(12) Manas-Zloczower, I. *Mixing and Compounding of Polymers*; Manas, I., Tadmor, Z., Eds.; Hanser Publishers: Munich, 1994.

(13) Vashisth, S.; Kumar, V.; Nigam, K. A Review on the Potential Application of curved Geometries in Process Industries. *Ind. Eng. Chem. Res.* **2008**, *47*, 3291−3337.

(14) Dean, W. Notes on the motion of fluid in a curved pipe. *Philos. Mag.* **1927**, *4*, 208−223.

(15) Dean, W. The stream line motion of fluid in a curved pipe. *Philos. Mag.* **1928**, *5*, 673−695.

(16) Adler, M. Flow in curved tubes. *Z. Angew. Math. Mech.* **1934**, *14*, 257−275.

(17) Kubair, V.; Kuloor, N. Heat transfer to Newtonian fluid in coiled pipes in laminar flow. *Int. J. Heat Mass Transfer* **1966**, *9*, 63−75.

(18) Shuchkin, V. Correlation for experimental data on heat transfer in curved pipes. *Therm Eng.* **1969**, *16*, 72−76.

(19) Dravid, A. N.; Smith, K. A.; Merrill, E. W.; Brian, P. L. T. Effect of secondary fluid motion on laminar flow heat transfer in helically coiled pipes. *AIChE J.* **1971**, *17*, 1114−1122.

(20) Kalb, C.; Seader, J. Heat and mass transfer phenomena for viscous flow in curved circular pipe. *Int. J. Heat Mass Transfer* **1972**, *15*, 801−817.

(21) Mishra, P.; Gupta, S. Momentum Transfer in Curved Pipes 1. Newtonian Fluids; 2. Non-Newtonian Fluids. *Ind. Eng. Chem. Process Des. Dev.* **1979**, *18*, 130−142.

(22) Ranade, V.; Ulbrecht, J. The residence time distribution for laminar flow of non-Newtonian liquids through helical tubes. *Chem. Eng. Commun.* **1981**, *8*, 165−176.

(23) Nigam, K.; Saxena, A. In *Encyclopedia of Fluid Mechanics*; Cheremisinoff, N. P., Ed.; Gulf Publishing: Houston, TX, 1986; Vol. *1*, Chapter 22, p 675.

(24) Kumar, V.; Gupta, P.; Nigam, K. Fluid Flow and Heat Transfer in Curved Tubes with Temperature dependent Properties. *Ind. Eng. Chem. Res.* **2007**, *46*, 3226−3236.

(25) Saxena, A.; Nigam, K. Axial dispersion in laminar flow of polymer solutions through coiled tubes. *J. Appl. Polym. Sci.* **1981**, *26*, 3475−3486.

(26) Nagy, A.; Faust, R.; Kennedy, J. Living carbocationic polymerization. *Polym. Bull.* **1986**, *15*, 411−416.

(27) Dowding, P.; Goodwin, J.; Vincent, B. Production of porous suspension polymers using a continuous tubular reactor. *Colloid Polym. Sci.* **2000**, *278*, 346−351.

(28) Cabral, P.; Melo, E.; Biscaia, P. A.; Lima, E.; Pinto, J. Free radical solution polymerization of styrene in a tubular reactor effects of recycling. *Polym. Eng. Sci.* **2003**, *43*, 1163.

(29) Rosenfeld, C.; Serra, C.; Brochon, C.; Hadziioannou, G. High temperature nitroxide mediated radical polymerization in a continuous microtube reactor: towards a better control of the polymerization reaction. *Chem. Eng. Sci.* **2007**, *62*, 5245−5250.

https://dx.doi.org/10.1021/acs.iecr.9b05142
Ind. Eng. Chem. Res. 2020, 59, 3854−3864

(30) Kumar, V.; Aggarwal, M.; Nigam, K. Mixing in curved tubes. *Chem. Eng. Sci.* **2006**, *61*, 5742−5753.
(31) Mansour, M.; Liu, Z.; Janiga, G.; Nigam, K.; Sundmacher, K.; Thévenin, D.; Zähringer, K. Numerical study of liquid-liquid mixing in helical pipes. *Chem. Eng. Sci.* **2017**, *172*, 250−261.
(32) Mansour, M.; Khot, P.; Thévenin, D.; Nigam, K.; Zähringer, K. Optimal Reynolds number for liquid-liquid mixing in helical pipes. *Chem. Eng. Sci.* **2020**, *214*, 114522.
(33) Mansour, M.; Thévenin, D.; Nigam, K.; Zähringer, K. Generally-valid optimal Reynolds and Dean numbers for efficient liquid-liquid mixing in helical pipes. *Chem. Eng. Sci.* **2019**, *201*, 382−385.
(34) Saxena, A. K.; Nigam, K. D. P. Nigam Coiled Configuration for Flow Inversion and its effect on Residence Time Distribution. *AIChE J.* **1984**, *30*, 363−368.
(35) Singh, J.; Verma, V.; Nigam, K. The Flow Characteristics of Power-Law Fluids in Coiled Flow Inverter. *Ind. Eng. Chem. Res.* **2013**, *52*, 207−221.
(36) Mridha, M.; Nigam, K. Coiled Flow Inverter as an Inline Mixer. *Chem. Eng. Sci.* **2008**, *63*, 1724−1732.
(37) Sharma, L.; Nigam, K.; Roy, S. Single phase mixing in coiled tubes and coiled flow inverters in different flow regimes. *Chem. Eng. Sci.* **2017**, *160*, 227−235.
(38) Zhou, Y.; Shah, S. Fluid flow in coiled tubing: a literature review and experimental investigation. *J. Can. Petrol Technol.* **2004**, *43*, 52−61.
(39) Naphon, P.; Wongwises, S. A review of flow and heat transfer characteristics in curved tubes. *Renewable Sustainable Energy Rev.* **2006**, *10*, 463−490.
(40) Mashelkar, R.; Devarajan, G. Secondary flows of non-Newtonian fluids: Part I laminar boundary layer flow of a generalized non Newtonian fluid in a coiled tube, Part II frictional losses in laminar flow of purely viscous and viscoelastic fluids through coiled tubes. *Trans. Inst. Chem. Eng.* **1976**, *54*, 100.
(41) Bowen, P.; Davies, A.; Walters, K. On viscoelastic effects in swirling flows. *J. Non-Newtonian Fluid Mech.* **1991**, *38*, 113.
(42) Joo, Y.; Shaqfeh, E. A purely elastic instability in Dean and Taylor-Dean flow. *Phys. Fluids A* **1992**, *4*, 524.
(43) Robertson, M.; Muller, S. Flow of Oldroyd-B fluids in curved pipes of circular and annular cross-section. *Int. J. Non-Linear Mech.* **1996**, *31*, 1−20.
(44) Saxena, A.; Nigam, K.; Nigam, K. Non- Newtonian Flow in Helical Coils - Diffusion Free RTD. *Can. J. Chem. Eng.* **1983**, *61*, 50−52.
(45) Singh, D.; Nigam, K. Laminar Dispersion of Polymer Solution in Helical Coils. *J. Appl. Polym. Sci.* **1981**, *26*, 785−790.
(46) Agrawal, S.; Jayaraman, G.; Srivastava, V. K.; Nigam, K. D. P. Power-Law Fluids in a Circular Curved Tubes, Part I Laminar Flow. *Polym.-Plast. Technol. Eng.* **1993**, *32*, 595−614.
(47) Agrawal, S.; Jayaraman, G.; Srivastava, V. K.; Nigam, K. D. P. Power-Law Fluids in a Circular Curved Tubes, Part II Laminar Axial Dispersion. *Polym.-Plast. Technol. Eng.* **1993**, *32*, 615−634.
(48) Agrawal, S.; Srivastava, V. K.; Jayaraman, G.; Nigam, K. D. P. Power-Law Fluids in a Circular Curved Tubes, Part III Numerical Simulation of Laminar Flow. *Polym.-Plast. Technol. Eng.* **1994**, *33*, 357−379.
(49) Mandal, M. M.; Serra, C.; Hoarau, Y.; Nigam, K. D. P. Numerical Modeling of Polystyrene in Coiled Flow inverter. *Microfluid. Nanofluid.* **2011**, *10*, 415−423.
(50) Bird, R. B.; Stewart, W. E.; Lightfoot, E. N. *Transport Phenomena*, 2nd ed.; John Wiley & Sons, Inc., 2006.
(51) Larson, R. G. *Constitutive Equations for Polymer Melts and Solutions*; Butterworths Series in Chemical Engineering; Elsevier, 1988.
(52) Galdi, G. P. In *Handbook of Mathematical Fluid Dynamics*; Friedlander, S. J., Serre, D., Eds.; Elsevier Science B.V., 2002; Vol. *1*; Chapter 7, pp 653−791.
(53) Favero, J.; Secchi, A.; Cardozo, N.; Jasak, H. Viscoelastic flow analysis using the software OpenFOAM and differential constitutive equations. *J. Non-Newtonian Fluid Mech.* **2010**, *165*, 1625−1636.
(54) Guénette, R.; Fortin, M. A new mixed finite element method for computing viscoelastic flows. *J. Non-Newtonian Fluid Mech.* **1995**, *60*, 27−52.
(55) Balci, N.; Thomases, B.; Renardy, M.; Doering, C. R. Symmetric factorization of the conformation tensor in viscoelastic fluid models. *J. Non-Newtonian Fluid Mech.* **2011**, *166*, 546−553.
(56) van Buel, R.; Schaaf, C.; Stark, H. Elastic turbulence in two-dimensional Taylor-Couette flows. *EPL (Europhysics Letters)* **2018**, *124*, 14001.
(57) Patankar, S. V.; Spalding, B. A calculation procedure for heat, mass and momentum transfer in three-dimensional parabolic flows. *Int. J. Heat Mass Transfer* **1972**, *15*, 1787−1806.
(58) Issa, R. I. Solution of the Implicitly Discretized Fluid Flow equations by Operator-Splitting. *J. Comput. Phys.* **1986**, *62*, 40−65.
(59) Holzmann, T. *Mathematics, Numerics, Derivations and OpenFOAM*; Holzmann CFD, 2016.
(60) Jasak, H. *OpenFOAM®: Selected Papers of the 11th Workshopp*; Springer, 2016.
(61) Hemingway, E. J.; Clarke, A.; Pearson, J. R. A.; Fielding, S. M. Thickening of viscoelastic flow in a model porous medium. *J. Non-Newtonian Fluid Mech.* **2018**, *251*, 56−68.
(62) Poole, R. The Deborah and Weissenberg numbers. *British Society of Rheology - Rheology Bulletin* **2012**, *53*, 32−39.
(63) Machado, A.; Bodiguel, H.; Beaumont, J.; Clisson, G.; Colin, A. Extra dissipation and flow uniformization due to elastic instabilities of shear-thinning polymer solutions in model porous media. *Biomicrofluidics* **2016**, *10*, 043507.
(64) Bodiguel, H.; Beaumont, J.; Machado, A.; Martinie, L.; Kellay, H.; Colin, A. Flow enhancement due to elastic turbulence in channel flows of shear thinning fluids. *Phys. Rev. Lett.* **2015**, *114*, 028302.
(65) Kukukova, A.; Aubin, J.; Kresta, S. M. A new definition of mixing and segregation: three dimensions of a key process variable. *Chem. Eng. Res. Des.* **2009**, *87*, 633−647.
(66) Alberini, F.; Simmons, M.J.H.; Ingram, A.; Stitt, E.H. Assessment of different methods of analysis to characterise the mixing of shear-thinning fluids in a Kenics KM static mixer using PLIF. *Chem. Eng. Sci.* **2014**, *112*, 152−169.
(67) Baddeley, A. *Analysing Spatial Point Patterns Workshop*, 2008. Obtained from: https://training.fws.gov/courses/references/tutorials/geospatial/CSP7304/documents/PointPatterTutorial.pdf.
(68) Diggle, P. *Statistical Analysis of Spatial Point Patterns*; Mathematics in Biology; Arnold, 2003.
(69) Diggle, P. J.; Matérn, B. On sampling designs for the study of point-event nearest neighbour distributions in R^2. *Scandinavian Journal of Statistics*, **200**780−84.
(70) Kukukova, A.; Aubin, J.; Kresta, S. Measuring the scale of segregation in mixing data. *Can. J. Chem. Eng.* **2011**, *89*, 1122−1138.
(71) Clark, P. J.; Evans, F. C. Distance to Nearest Neighbor as a Measure of Spatial Relationships in opulations. *Ecology* **1954**, *35*, 445−453.
(72) Acharya, N.; Sen, M.; Chang, H.-C. Analysis of heat transfer enhancement in coiled-tube heat exchangers. *Int. J. Heat Mass Transfer* **2001**, *44*, 3189−3199.
(73) White, C. Streamline flow through curved pipes. *Proc. R. Soc. London A* **1929**, *123*, 645−663.
(74) Pimenta, T.; Campos, J. Friction losses of Newtonian and non-Newtonian fluids flowing in laminar regime in a helical coil. *Exp. Therm. Fluid Sci.* **2012**, *36*, 194−204.

https://dx.doi.org/10.1021/acs.iecr.9b05142
Ind. Eng. Chem. Res. 2020, 59, 3854−3864